EUROPEAN ORGANIZATION FOR NUCLEAR RESEARCH

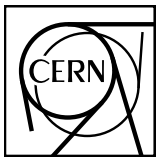

ALICE-PUBLIC-2022-010

Physics Preliminary Summary: Measurement of beauty-strange meson production in Pb–Pb collisions at $\sqrt{s_{\rm NN}} = 5.02$ TeV via non-prompt $\rm D_s^+$ mesons

ALICE Collaboration

Abstract

The production yields of non-prompt $\rm D_s^+$ mesons, namely $\rm D_s^+$ mesons from beauty-hadron decays, were measured for the first time as a function of the transverse momentum ($p_{\rm T}$) at midrapidity ($|y| < 0.5$) in central and semi-central Pb–Pb collisions at a centre-of-mass energy per nucleon pair $\sqrt{s_{\rm NN}} = 5.02$ TeV with the ALICE experiment at the LHC. The $\rm D_s^+$ mesons and their charge conjugates were reconstructed from the hadronic decay channel $\rm D_s^+ \rightarrow \phi\pi^+$, with $\phi \rightarrow \rm K^-K^+$, in the $4 < p_{\rm T} < 36$ GeV/c and $2 < p_{\rm T} < 24$ GeV/c intervals for the 0–10% and 30–50% centrality classes, respectively. The measured yields of non-prompt $\rm D_s^+$ mesons are compared to those of prompt $\rm D_s^+$ and non-prompt $\rm D^0$ mesons by calculating the ratios of the production yields in Pb–Pb collisions and the nuclear modification factor $R_{\rm AA}$. The ratio between the $R_{\rm AA}$ of non-prompt $\rm D_s^+$ and prompt $\rm D_s^+$ mesons, and that between the $R_{\rm AA}$ of non-prompt $\rm D_s^+$ and non-prompt $\rm D^0$ mesons in central Pb–Pb collisions are found to be on average higher than unity in the $4 < p_{\rm T} < 12$ GeV/c interval with a statistical significance of about $1.6\,\sigma$ and $1.7\,\sigma$, respectively. The measured $R_{\rm AA}$ ratios are compared with the predictions of theoretical models of heavy-quark transport in a hydrodynamically expanding QGP that incorporate hadronisation via quark recombination.

1 Introduction

A transition from ordinary nuclear matter to a colour-deconfined medium called quark–gluon plasma (QGP) is predicted to occur at a very high temperature and energy density by quantum chromodynamics (QCD) calculations on the lattice [1–3], and is supported by several measurements in ultrarelativistic heavy-ion collisions at the SPS, RHIC, and LHC [4–11]. In such collisions, charm and beauty quarks are mainly produced in hard scattering processes that occur before the formation of the QGP. Hence, they are effective probes of the entire system evolution. While the system undergoes a hydrodynamic expansion, they interact with the medium constituents via elastic [12–14] and inelastic [15, 16] scatterings. These interactions imply that charm and beauty quarks exchange energy and momentum with the medium constituents, causing high-momentum quarks to lose part of their energy while traversing the QGP. The in-medium energy loss is commonly studied via the measurement of the nuclear modification factor,

$$R_{\rm AA}(p_{\rm T}) = \frac{1}{\langle T_{\rm AA}\rangle} \times \frac{{\rm d}N_{\rm AA}/{\rm d}p_{\rm T}}{{\rm d}\sigma_{\rm pp}/{\rm d}p_{\rm T}}, \tag{1}$$

where ${\rm d}N_{\rm AA}/{\rm d}p_{\rm T}$ is the transverse-momentum ($p_{\rm T}$) differential production yield in nucleus–nucleus collisions, ${\rm d}\sigma_{\rm pp}/{\rm d}p_{\rm T}$ the $p_{\rm T}$-differential cross section in proton–proton (pp) collisions, and $\langle T_{\rm AA}\rangle$ the average of the nuclear overlap function [17]. Several measurements of charm and beauty hadrons in Pb–Pb [18–28] and Au–Au [29] collisions show a strong suppression of the production yield at intermediate and high $p_{\rm T}$ ($p_{\rm T} > 4$–5 GeV/c) in heavy-ion collisions compared to pp collisions, suggesting a substantial energy loss of heavy quarks in the QGP. The comparison of the $R_{\rm AA}$ of light, charm, and beauty hadrons indicates that the energy loss is sensitive to the colour charge and the parton mass. In particular, the $R_{\rm AA}$ of beauty hadrons is observed to be larger than that of charm hadrons [21, 24]. For $p_{\rm T} > 5$–6 GeV/c, where radiative processes are expected to dominate the energy loss, the smaller suppression is attributed mainly to the so-called "dead cone" effect [30, 31], which suppresses the gluon radiation at angles smaller than $\theta \approx m_{\rm Q}/E_{\rm Q}$, where $m_{\rm Q}$ is the mass of the quark and $E_{\rm Q}$ its energy.

Instead, low-$p_{\rm T}$ heavy quarks experience a "Brownian motion", which consists of a diffusion process occurring via multiple elastic interactions with low-momentum transfer [32]. Owing to the larger mass, beauty quarks diffuse less than charm quarks and have a longer relaxation time, which is expected to be proportional to the quark mass. Measurements of the heavy-flavour hadron production and azimuthal anisotropies can be exploited to constrain the spatial diffusion coefficient D_s via the comparison with theoretical models based on the heavy-quark transport in a hydrodynamically expanding QGP [18, 33].

A precise description of the hadronisation process in the hot nuclear matter is crucial to understand the transport properties of the QGP [34]. The hadronisation mechanism of low and intermediate-$p_{\rm T}$ heavy quarks is expected to be sensitive to the presence of a colour-deconfined medium, which could enable hadron formation via quark recombination in addition to the vacuum-like fragmentation. This leads to an enhancement of the production yield of heavy-flavour hadrons with strange-quark content relative to those of non-strange hadrons in Pb–Pb collisions compared to pp collisions, caused by the abundant production of strange–antistrange quark pairs in the QGP [11, 35, 36]. Recent measurements of the production of prompt $\rm D_s^+$ mesons, i.e. $\rm D_s^+$ mesons originating from the charm-quark hadronisation or decays of excited charm-hadron states, by the STAR [37] and ALICE [19, 38] Collaborations suggest a relevant role of the recombination mechanism in the charm-quark hadronisation. Similar studies in the open-beauty sector, conducted by the CMS Collaboration via the measurement of the $\rm B_s^0$-meson production relative to that of $\rm B^+$ mesons, show a hint of enhanced production of strange over non-strange mesons [26, 39]. However, no firm conclusions can be drawn within the current uncertainties. Complementary information about the heavy-quark hadronisation in presence of the medium is provided by the measurements of charm baryons and charmonia in heavy-ion collisions [20, 27, 40–43].

In this Note, the measurement of the production of $\rm D_s^+$ mesons originating from beauty-hadron decays (non-prompt) is reported for central (0–10%) and semicentral (30–50%) Pb–Pb collisions at a centre-of-

mass energy per nucleon pair $\sqrt{s_{\mathrm{NN}}} = 5.02$ TeV. Non-prompt $\mathrm{D_s^+}$ mesons provide information about the diffusion and the energy loss of beauty quarks in the QGP. In addition, together with the measurement of non-prompt $\mathrm{D^0}$ mesons, they have the potential to reveal the beauty-quark hadronisation mechanisms in the QGP, since in pp collisions about 50% of non-prompt $\mathrm{D_s^+}$ mesons are produced in $\mathrm{B_s^0}$ decays [44, 45]. Therefore, the non-prompt $\mathrm{D_s^+}$ p_{T}-differential production yield and R_{AA} are compared with those of prompt $\mathrm{D_s^+}$ and non-prompt $\mathrm{D^0}$ mesons, as well as with theoretical models based on beauty-quark transport in the QGP.

2 Experimental apparatus and analysis technique

The $\mathrm{D_s^+}$-mesons were reconstructed from their hadronic decays with the ALICE central barrel detectors, which cover the full azimuth in the pseudorapidity interval $|\eta| < 0.9$ and are embedded in a large solenoidal magnet providing a uniform 0.5 T magnetic field parallel to the beam direction. Charged-particle trajectories are reconstructed from their hits in the Inner Tracking System (ITS) [46] and the Time Projection Chamber (TPC) [47]. Particle identification (PID) is provided via the measurement of the specific ionisation energy loss $\mathrm{d}E/\mathrm{d}x$ in the TPC and of the flight time of the particles from the interaction point to the Time-Of-Flight detector (TOF) [48]. The reconstruction of the interaction vertex and of the decay vertices of charm- and beauty-hadron decays relies on the precise determination of the track parameters in the vicinity of the interaction point provided by the ITS.

The data sample of Pb–Pb collisions used in the analysis was collected with the ALICE detector in 2018, during LHC Run 2. Three trigger classes were considered: minimum bias, central, and semicentral, all based on the signals in the two scintillator arrays of the V0 detector [49], which covers the full azimuth in the pseudorapidity intervals $-3.7 < \eta < -1.7$ (V0C) and $2.8 < \eta < 5.1$ (V0A). Background events due to the interaction of one of the beams with residual gas in the vacuum tube and other machine-induced backgrounds were rejected offline using the timing information provided by the V0 and the neutron Zero Degree Calorimeters (ZDC) [50]. Only events with a primary vertex reconstructed within ± 10 cm from the centre of the detector along the beam-line direction were considered in the analysis. Collisions were classified into centrality intervals, defined in terms of percentiles of the hadronic Pb–Pb cross section, based on the V0 signal amplitude as described in detail in Ref. [51]. The measurement of non-prompt $\mathrm{D_s^+}$-meson production was carried out for central (0–10%) and semicentral (30–50%) collisions. The number of events considered for the analysis is about 100×10^6 and 85×10^6 in the 0–10% and 30–50% centrality intervals, corresponding to integrated luminosities $\mathscr{L}_{\mathrm{int}}$ of (130.5 ± 0.5) $\mu\mathrm{b}^{-1}$ and (55.5 ± 0.2) $\mu\mathrm{b}^{-1}$, respectively [52]. The average values of the nuclear overlap function, $\langle T_{\mathrm{AA}} \rangle$, for the considered central and semicentral event intervals were estimated via Glauber-model [53] simulations anchored to the V0 signal amplitude distribution, and are (23.26 ± 0.17) mb^{-1} and (3.92 ± 0.06) mb^{-1} [17, 52], respectively.

The $\mathrm{D_s^+}$ mesons and their charge conjugates were reconstructed via the $\mathrm{D_s^+} \to \phi\pi^+ \to \mathrm{K^-K^+}\pi^+$ decay channel with branching ratio $\mathrm{BR} = (2.24 \pm 0.08)\%$ [44]. The analysis was based on the reconstruction of decay-vertex topologies displaced from the interaction vertex. For prompt mesons, the separation between the interaction point and the $\mathrm{D_s^+}$ decay vertex is governed by the mean proper decay length $c\tau$ of $\mathrm{D_s^+}$ mesons, which is about 151 μm [44]. The decay vertices of non-prompt $\mathrm{D_s^+}$ mesons on average are more displaced than those of prompt $\mathrm{D_s^+}$ mesons due to the large mean proper decay lengths of beauty hadrons ($c\tau \simeq 450$ μm [44]). Therefore, by exploiting the selection of displaced decay-vertex topologies, it is possible to separate non-prompt $\mathrm{D_s^+}$ mesons from the combinatorial background and from prompt $\mathrm{D_s^+}$ mesons.

$\mathrm{D_s^+}$-meson candidates were built combining triplets of tracks with the proper charge signs, each with $|\eta| < 0.8$, at least 70 (out of a maximum of 159) crossed TPC pad rows, a track fit quality $\chi^2/\mathrm{ndf} < 1.25$ in the TPC (where ndf is the number of degrees of freedom involved in the track fit procedure), and a

minimum of two (out of a maximum of six) hits in the ITS, with at least one in either of the two innermost layers, which provide the best pointing resolution. Moreover, at least 50 clusters available for particle identification in the TPC were required, and only tracks with p_{T} above 0.6 (0.4) GeV/c were considered for central (semicentral) collisions. These track selection criteria limit the $\mathrm{D_s^+}$-meson acceptance in rapidity, which drops steeply to zero for $|y| > 0.5$ at low p_{T} and for $|y| > 0.8$ at $p_{\mathrm{T}} > 5$ GeV/c. Thus, only $\mathrm{D_s^+}$-meson candidates within a p_{T}-dependent fiducial acceptance region, $|y| < y_{\mathrm{fid}}(p_{\mathrm{T}})$, were selected. The $y_{\mathrm{fid}}(p_{\mathrm{T}})$ value was defined as a second-order polynomial function, increasing from 0.5 to 0.8 in the transverse-momentum range $0 < p_{\mathrm{T}} < 5$ GeV/c, and as a constant term, $y_{\mathrm{fid}} = 0.8$, for $p_{\mathrm{T}} > 5$ GeV/c.

Similarly to other recent D-meson measurements by the ALICE Collaboration [19, 21, 45], Boosted Decision Trees (BDT) algorithms were employed to reduce the large combinatorial background and to separate the contribution of prompt and non-prompt $\mathrm{D_s^+}$ mesons through a multiclass classification. In particular, the implementation of the BDT algorithm provided by the XGBoost [54, 55] library was used. Background samples for the BDT training were extracted from the sidebands of the candidate invariant mass distributions in the data, namely from the $1.72 < M(\mathrm{KK}\pi) < 1.83$ GeV/c^2 and $2.01 < M(\mathrm{KK}\pi) < 2.12$ GeV/c^2 regions. Applying these selections, candidates belonging to $\mathrm{D^+ \to K^-K^+\pi^+}$ decays are rejected. Signal samples of prompt and non-prompt $\mathrm{D_s^+}$ mesons were obtained from Monte Carlo (MC) simulations. The MC samples were built by simulating Pb–Pb collisions with the HIJING 1.36 [56] event generator in order to describe the charged-particle multiplicity and detector occupancy. To enrich the sample of prompt and non-prompt D-meson signals, additional $\mathrm{c\overline{c}}$- and $\mathrm{b\overline{b}}$-quark pairs were injected into each HIJING event using the PYTHIA 8.243 event generator [57, 58] with Monash tune [59]. The $\mathrm{D_s^+}$ mesons were forced to decay into the hadronic channel of interest for the analysis. The generated particles were then propagated through the apparatus using the GEANT3 transport code [60]. Detailed descriptions of the detector response, the geometry of the apparatus and the conditions of the luminous region, including their evolution with time during the data taking period, were included in the simulation. Before the BDT training, loose kinematic and topological selections were applied to the $\mathrm{D_s^+}$-meson candidates together with the particle identification of decay-product tracks. The $\mathrm{D_s^+}$-meson candidate information provided to the BDTs, as an input for the models to distinguish among prompt and non-prompt mesons and background candidates, was mainly based on the displacement of the tracks from the primary vertex, the distance between the $\mathrm{D_s^+}$-meson decay vertex and the primary vertex, the $\mathrm{D_s^+}$-meson impact parameter, and the cosine of the pointing angle between the $\mathrm{D_s^+}$-meson candidate line of flight (the vector connecting the primary and secondary vertices) and its reconstructed momentum vector. In addition, the absolute difference between the reconstructed $\mathrm{K^+K^-}$ invariant mass and the PDG average mass for the ϕ meson [44] and variables related to the PID of decay tracks were also included. Independent BDTs were trained in the different p_{T} intervals of the analysis and for the different centrality intervals. Subsequently, they were applied to the real data sample in which the type of candidate is unknown. The BDT outputs are related to the candidate probability to be a non-prompt $\mathrm{D_s^+}$ meson or combinatorial background. Selections on the BDT outputs were optimised to obtain a high non-prompt $\mathrm{D_s^+}$-meson fraction while maintaining a reliable signal extraction from the candidate invariant mass distributions.

The $\mathrm{D_s^+}$-meson candidates were selected by requiring a high probability to be non-prompt $\mathrm{D_s^+}$ mesons and a low probability to be combinatorial background. The raw yield of $\mathrm{D_s^+}$ mesons, including both particles and antiparticles, was extracted from binned maximum-likelihood fits to the invariant mass (M) distributions in transverse-momentum intervals $4 < p_{\mathrm{T}} < 36$ GeV/c and $2 < p_{\mathrm{T}} < 24$ GeV/c for the 0–10% and the 30–50% centrality intervals, respectively. The fit function was composed of a Gaussian for the description of the signal and an exponential term for the background. An additional Gaussian was used to describe the peak due to the decay $\mathrm{D^+ \to K^-K^+\pi^+}$, with a branching ratio of $(9.68 \pm 0.18) \times 10^{-3}$ [44], present at a lower invariant mass value than the $\mathrm{D_s^+}$-meson signal peak. To improve the stability of the fits, the width of the $\mathrm{D_s^+}$-meson signal peak was fixed to the value extracted from a data sample dominated by prompt candidates, which is characterised by a signal extraction with

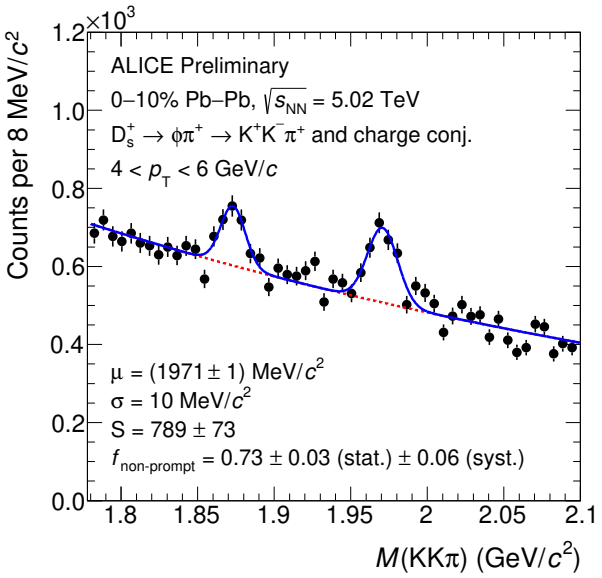

Fig. 1: Invariant mass distribution of non-prompt D_s^+ candidates and their charge conjugates in the $4 < p_T < 6$ GeV/c interval for central Pb–Pb collisions. The blue solid line shows the total fit function and the red dashed line the combinatorial-background contribution. The values of the mean (μ), width (σ), and raw yield (S) of the signal peak are reported together with their statistical uncertainties resulting from the fit. The fraction of non-prompt candidates in the measured raw yield is reported with its statistical and systematic uncertainties.

higher statistical significance. As an example, the invariant mass distribution for the $4 < p_T < 6$ GeV/c interval in central Pb–Pb collisions, together with the result of the fit and the estimated non-prompt fraction is reported in Fig. 1. The measured raw yield, although dominated by non-prompt candidates, still contains a residual contribution of prompt D_s^+ mesons which satisfy the BDT-based selections. The procedure used to calculate the fraction of non-prompt candidates present in the extracted raw yield is described below. The statistical significance of the observed signals varies from about 4 to 11 depending upon the p_T and centrality intervals.

The corrected p_T-differential yields of non-prompt D_s^+ mesons were computed for each p_T interval as

$$\left.\frac{dN}{dp_T}\right|_{|y|<0.5} = \frac{1}{2} \times \frac{1}{\Delta p_T} \times \frac{f_{\text{non-prompt}}(p_T) \times N^{D+\overline{D},\text{raw}}(p_T)\Big|_{|y|<y_{\text{fid}}(p_T)}}{c_{\Delta y}(p_T) \times (\text{Acc} \times \varepsilon)_{\text{non-prompt}}(p_T) \times \text{BR} \times N_{\text{evt}}} . \quad (2)$$

The raw-yield values $N^{D+\overline{D},\text{raw}}$ were divided by a factor of two and multiplied by the non-prompt fraction $f_{\text{non-prompt}}$ to obtain the charge-averaged yields of non-prompt D_s^+ mesons. Furthermore, they were divided by the acceptance-times-efficiency correction factor of non-prompt D_s^+ mesons $(\text{Acc} \times \varepsilon)_{\text{non-prompt}}$, the BR of the decay channel, the width of the p_T interval Δp_T, the correction factor for the rapidity coverage $c_{\Delta y}$, and the number of analysed events N_{evt}. The correction factor for the rapidity acceptance $c_{\Delta y}$ was defined as the ratio between the generated D-meson yield in $\Delta y = 2\, y_{\text{fid}}(p_T)$ and that in $|y| < 0.5$. It was computed with FONLL perturbative QCD calculations [61, 62] as in Refs. [18, 19].

The $(\text{Acc} \times \varepsilon)$ correction factor was obtained from MC simulations, using samples not employed in the BDT training. The D_s^+-meson p_T distributions from simulations were reweighed in order to mimic the realistic shapes in the determination of the $(\text{Acc} \times \varepsilon)$ factor, which depends on p_T. In particular, weights were applied to the p_T distributions of prompt D_s^+ mesons and of beauty-hadron mother particles in case of non-prompt D_s^+ mesons. These weights were defined to reproduce the shapes given by FONLL calculations multiplied by the R_{AA} of prompt D_s^+ mesons and B mesons predicted by the TAMU [63] model. The TAMU model implements the charm- and beauty-quark transport inside a strangeness-rich

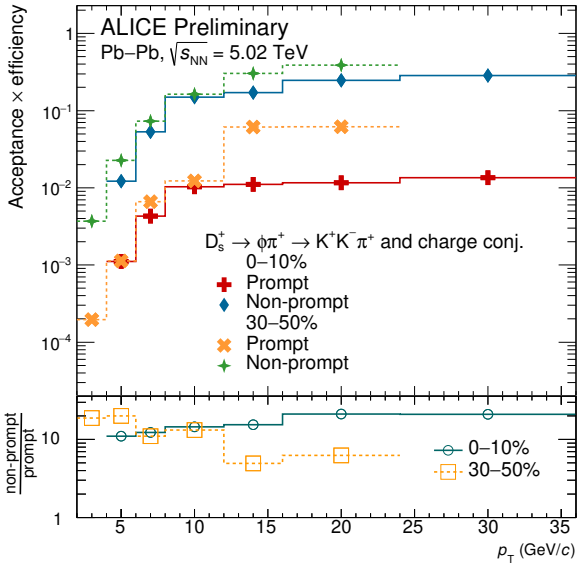

Fig. 2: Acceptance-times-efficiency factors for prompt and non-prompt D_s^+ mesons as a function of p_T in the 0–10% and 30–50% centrality intervals, together with their ratios (bottom panel).

QGP, and it reasonably reproduces the prompt D-meson measurements at low p_T [18, 19]. The $(\mathrm{Acc} \times \varepsilon)$ factors as a function of p_T for prompt and non-prompt D_s^+ mesons in the 0–10% and 30–50% centrality intervals are displayed in Fig. 2, along with the ratios of the non-prompt to prompt factors. The prompt D_s^+-meson acceptance times efficiency is smaller than that of non-prompt D_s^+ mesons by a factor varying from 5 to 20 depending on p_T and centrality. This is expected since the selections applied to obtain the non-prompt enriched sample strongly suppress the prompt D_s^+-meson efficiency. Instead, the acceptance is the same for prompt and non-prompt mesons. In central collisions, the prompt D_s^+-meson suppression increases with increasing p_T. The opposite trend is observed in semicentral collisions, since less stringent selections on the BDT outputs are necessary to extract the non-prompt D_s^+-meson signal due to the lower yield.

The fraction $f_{\text{non-prompt}}$ of non-prompt D_s^+ mesons in the extracted raw yield was estimated with a data-driven procedure based on the construction of data samples with different abundances of prompt and non-prompt candidates. These samples were built by varying the selection on the BDT output related to the candidate probability to be a non-prompt D_s^+ meson. Starting from the values of raw yield and acceptance times efficiency of prompt and non-prompt D_s^+ mesons obtained for each sample, the corrected yield of prompt and non-prompt D_s^+ mesons and the $f_{\text{non-prompt}}$ fraction were calculated. This data-driven technique does not depend on theoretical calculations of heavy-quark production and interaction with the QGP constituents, and it is described in detail in Ref. [45]. The $f_{\text{non-prompt}}$ fractions obtained as a function of p_T in central and semicentral Pb–Pb collisions are reported in Fig. 3, together with their statistical and systematic uncertainties. The determination of the systematic uncertainty on the $f_{\text{non-prompt}}$ fraction is described in Section 3. The $f_{\text{non-prompt}}$ values vary between about 0.72 (0.56) and 0.82 (0.70) in the 0–10% (30–50%) centrality interval as a function of transverse momentum. The $f_{\text{non-prompt}}$ is observed to be on average lower in semicentral collision with respect to central collisions. This difference is expected as in the 30–50% centrality interval less stringent BDT selections were applied compared to 0–10% centrality interval.

The non-prompt D_s^+-meson nuclear modification factor, R_{AA}, was computed according to Eq. 1. The measurement of the p_T-differential cross section of non-prompt D_s^+ mesons at midrapidity ($|y| < 0.5$) in pp collisions at $\sqrt{s} = 5.02$ TeV from Ref. [45], which covers the transverse-momentum interval $2 < p_T < 12$ GeV/c, was used as the reference for the R_{AA} computation. For $p_T > 12$ GeV/c, an

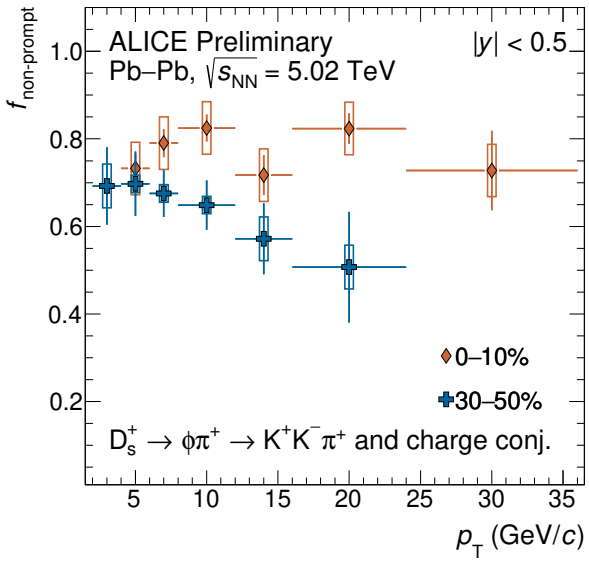

Fig. 3: Fraction of non-prompt D_s^+ mesons in the extracted raw yield as a function of p_T in the 0–10% and 30–50% centrality intervals. The vertical bars (boxes) report the statistical (systematic) uncertainties.

extrapolated pp reference was obtained from FONLL calculations of the beauty-hadron cross section and by using PYTHIA 8 to describe the decay kinematics of beauty hadrons to D_s^+ mesons, for more details see Ref. [45]. The resulting predictions were then scaled to match the measured values at lower transverse momenta. The total systematic uncertainty on the pp reference is $^{+38}_{-28}$% for all the extrapolated p_T intervals. The procedures for the p_T extrapolation and the systematic uncertainty estimation are the same as in Ref. [64].

3 Systematic uncertainties

The following sources of systematic uncertainty were considered for the production yield and R_{AA} estimation: (i) the raw-yield extraction, (ii) track reconstruction efficiency, (iii) non-prompt D_s^+-meson fraction, (iv) BDT selection efficiency, (v) PID selection efficiency, (vi) relative abundances of beauty-hadron species in the MC simulation, and (vii) shapes of the simulated p_T-differential distributions. The resulting systematic uncertainties on the non-prompt D_s^+-meson yield and R_{AA} in representative p_T intervals are summarised in Table 1. In the R_{AA} computation, the systematic uncertainties on the pp measurement were treated as uncorrelated from the ones on the Pb–Pb corrected yields, except for the uncertainty on the BR (3.6%) [44] which cancels in the R_{AA} and was considered only in the p_T-differential production yield. The normalisation uncertainty on the R_{AA} includes the uncertainty on the integrated luminosity in pp collisions (2.1% [65]), the uncertainty on the $\langle T_{AA} \rangle$ estimation, 0.7% (1.5%) for the 0–10% (30–50%) centrality interval [17], and the one related to the centrality-interval definition. This last contribution is due to the uncertainty on the fraction of the hadronic cross section used in the Glauber fit to determine the centrality. It was estimated to be < 0.1% and 2% for the 0–10% and 30–50% centrality intervals, respectively [64].

The systematic uncertainty on the raw-yield extraction was estimated by adopting several fit configurations changing the background fit function (linear and parabolic), the upper and lower fit limits, and the bin size of the invariant mass spectrum. The sensitivity to the line shape of the D_s^+ peak was tested by comparing the raw-yield values from the fits with those obtained by counting the candidates in the invariant mass region of the signal after subtracting the background estimated from the side bands.

The systematic uncertainty on the track reconstruction efficiency accounts for possible discrepancies

between data and MC in the ITS–TPC prolongation efficiency and in the selection efficiency due to track-quality criteria in the TPC. The per-track systematic uncertainties were estimated by varying the track-quality selection criteria and by comparing the prolongation probability of the TPC tracks to the ITS hits in data and simulations. They were then propagated to the non-prompt $\mathrm{D_s^+}$ mesons via their decay kinematics.

The systematic uncertainties on the non-prompt $\mathrm{D_s^+}$-meson fraction and the BDT selection efficiency are due to possible discrepancies between data and MC in the distributions of the variables used in the BDT-model training (i.e. the $\mathrm{D_s^+}$-meson decay-vertex topology, kinematic, and PID variables). The former was computed by varying the configuration and the number of BDT selections employed in the data-driven method described in Sec. 2. In particular, wider and narrower intervals of the probability to be non-prompt $\mathrm{D_s^+}$ mesons, and smaller and larger step sizes between the chosen BDT selections were considered. For each configuration, the non-prompt $\mathrm{D_s^+}$-meson fraction was recomputed. Instead, the systematic uncertainty related to the BDT selection efficiency was studied by repeating the entire analysis varying the selection criteria based on the BDT outputs. The uncertainty for this source of systematic uncertainty was assigned considering the RMS and the shift of the correct yield obtained by varying the BDT selection with respect to the reference one.

Analogously, the systematic uncertainty on the PID selection efficiency relative to the loose selection on the PID variables applied before the BDT ones was also considered. This source was evaluated in the prompt $\mathrm{D_s^+}$-meson analysis [19], and it was found to be negligible for the adopted PID strategy.

The selection efficiency of non-prompt $\mathrm{D_s^+}$ mesons originating from the decay of different beauty-hadron species can differ because of the different lifetime of the parent hadron and the different decay kinematics. Consequently, an imperfect description in the MC simulation of the beauty-hadron composition might result in a bias in the estimation of the D-meson efficiencies. This is especially important for $\mathrm{D_s^+}$ mesons, which receive significant contributions from all the three ground-state B-meson species ($\mathrm{B^+}$, $\mathrm{B^0}$, and $\mathrm{B_s^0}$). The PYTHIA 8 event generator describes the measurements of different B-meson species in pp collisions [45], however in heavy-ion collisions an enhanced production of strange over non-strange B mesons is expected compared to the one observed in pp collisions. Nevertheless, since no precise measurement of $\mathrm{B_s^0}$-meson production down to low momentum is available in Pb–Pb collisions, the relative abundances present in PYTHIA 8 were used without applying any reweighting. The systematic uncertainty introduced by this assumption was estimated by reweighting the $\mathrm{B_s^0}$ contribution present in the MC enhanced by a factor 2 as predicted by the TAMU model [66]. The systematic uncertainty was assigned considering the variation between the production yield estimated using the enhanced $\mathrm{B_s^0}$ contribution and the default one.

The systematic uncertainty due to the shape of the p_{T} distributions of $\mathrm{D_s^+}$ mesons and beauty hadrons in the MC simulations was evaluated by applying different weights to the p_{T} distributions of prompt $\mathrm{D_s^+}$ mesons and of beauty-hadron mother particles in case of non-prompt $\mathrm{D_s^+}$ mesons. As an alternative to the TAMU model, the shape resulting from the LIDO model [67] was considered. The main difference between the TAMU and LIDO model derives from the fact that the former includes the enhanced production of the $\mathrm{B_s^0}$ mesons, unlike the latter. The systematic uncertainty was assigned considering the variation of the corrected yield compared to the default case.

4 Results

Figure 4 shows the p_{T}-differential production yield of prompt and non-prompt $\mathrm{D_s^+}$ mesons in central and semicentral Pb–Pb collisions at $\sqrt{s_{\mathrm{NN}}} = 5.02$ TeV. The measured prompt $\mathrm{D_s^+}$-meson production yields were taken from Ref. [19] and scaled by a factor 10 for visibility.

Figure 5 reports the ratios of the production yield of non-prompt to prompt $\mathrm{D_s^+}$ (left panel) and non-

Table 1: Systematic uncertainties on the measurement of the non-prompt D_s^+-meson corrected yield and R_{AA} in the 0–10% and 30–50% centrality intervals for representative transverse-momentum intervals.

Centrality interval	0–10%		30–50%	
p_T (GeV/c)	2–4	12–16	2–4	12–16
Yield extraction	10%	5%	10%	5%
Tracking efficiency	12%	13%	11%	12%
Non-prompt fraction	12%	6%	5%	6%
Selection efficiency	12%	5%	10%	5%
PID efficiency	negl.	negl.	negl.	negl.
B hadrochemistry	1%	1%	1%	1%
MC p_T shape	20%	8%	15%	2%
Centrality limits	< 0.1%		2%	
$\langle T_{AA} \rangle$	0.7%		1.5%	
$\mathscr{L}_{int}^{pp}$	2.1%			
Branching ratio	3.6%			

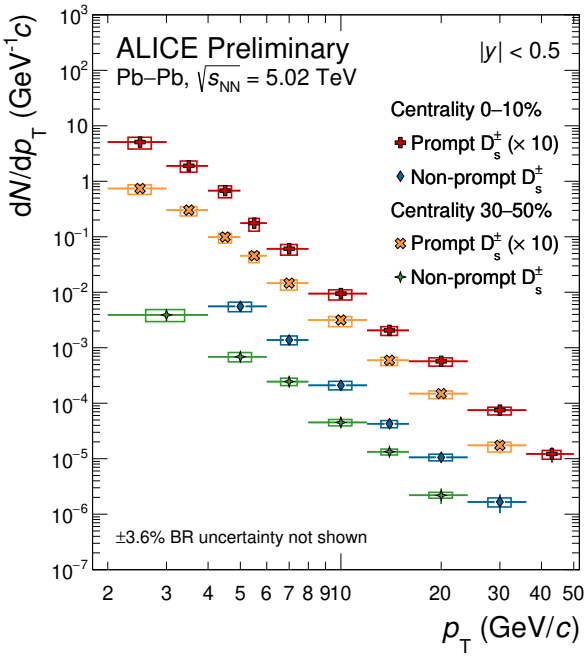

Fig. 4: Prompt and non-prompt D_s^+ meson production yield in central and semicentral Pb–Pb collisions at $\sqrt{s_{NN}} = 5.02$ TeV. The prompt D_s^+ results are taken from Ref. [19] and scaled by a factor 10 for visibility. The vertical bars (boxes) report the statistical (systematic) uncertainties.

prompt D_s^+ to non-prompt D^0 [21] (right panel) in central and semicentral Pb–Pb collisions, as well as in pp collisions [45]. Computing these ratios helps to further investigate the effects of the QGP medium on the hadron formation mechanism. To get an indication of the B_s^0-meson p_T probed by non-prompt D_s^+ mesons, a simulation with PYTHIA 8 was performed. As an example, the mean p_T distribution of B_s^0 mesons decaying to D_s^+ mesons with $4 < p_T < 6$ GeV/c has a mean of about 8.8 GeV/c and an RMS of about 3.1 GeV/c. The non-prompt to prompt D_s^+-meson ratio ranges between about 0.05 and 0.20 and increases with increasing p_T up to $p_T = 10$ GeV/c. At higher momentum the slope of the ratios seems to reduce, even though no firm conclusions can be drawn with the current uncertainties. On the other

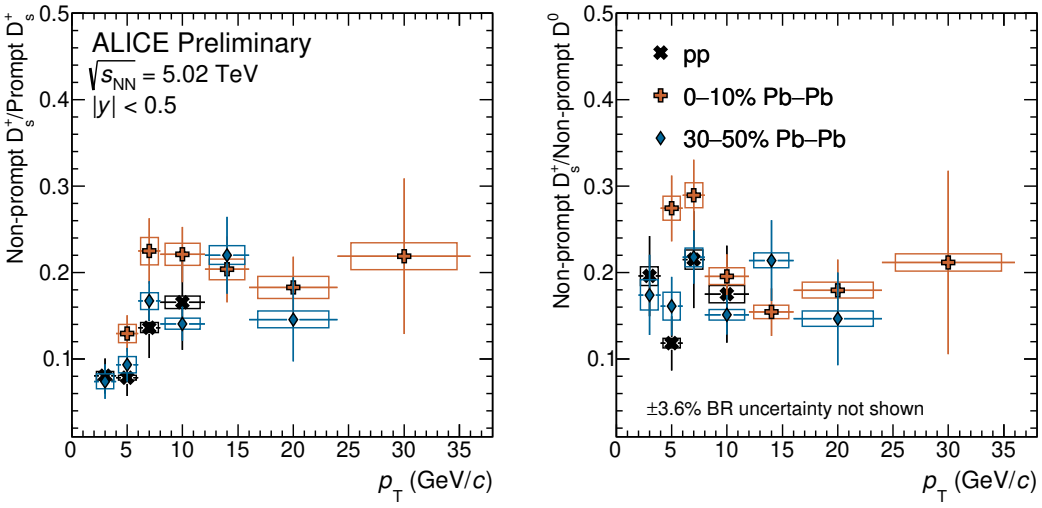

Fig. 5: The p_{T}-differential production yield of non-prompt $\mathrm{D_s^+}$ mesons divided by those of prompt $\mathrm{D_s^+}$ mesons (left panel) and non-prompt $\mathrm{D^0}$ mesons (right panel) for the 0–10% and 30–50% centrality intervals in Pb–Pb collisions at $\sqrt{s_{\mathrm{NN}}} = 5.02$ TeV from Refs. [19, 21] compared with those in pp collisions at the same centre-of-mass energy from Ref. [45].

hand, the non-prompt $\mathrm{D_s^+}$ to non-prompt $\mathrm{D^0}$ ratio shows an almost flat trend around 0.2 in the p_{T} range of the measurement. The ratios computed in pp and semicentral Pb–Pb collisions are compatible within the uncertainties. A hint of enhancement compared to pp collisions with a significance of 1.7σ, where σ indicates the sum in quadrature of statistical and systematic uncertainties, is found by performing a weighted average of the non-prompt $\mathrm{D_s^+/D^0}$ values in the $4 < p_{\mathrm{T}} < 12$ GeV/c interval for the 0–10% centrality class. The inverse of the squared sum of the relative statistical and p_{T}-uncorrelated systematic uncertainties was used as weight in the average. All the systematic uncertainties, except for those on the raw-yield extraction, were considered as fully correlated in p_{T}. This hint of a larger non-prompt $\mathrm{D_s^+/D^0}$ yield ratio is consistent with an enhanced production of strange-beauty mesons in heavy-ion collisions compared to pp collisions, as expected in a scenario in which beauty quarks hadronise via recombination with surrounding quarks in the strangeness-enriched QGP medium. In the transverse-momentum interval $4 < p_{\mathrm{T}} < 12$ GeV/c, also the non-prompt to prompt $\mathrm{D_s^+}$-meson ratio in the 0–10% centrality class shows a mild enhancement with respect to pp collisions with a significance of 1.6σ.

The R_{AA} of non-prompt $\mathrm{D_s^+}$ mesons was computed according to Eq. 1, where the pp reference was obtained from the measurement published in Ref. [45]. To study the effects of the QGP medium on the resulting momentum spectra and the hadronisation mechanism of beauty quarks, the nuclear modification factor measured for the non-prompt $\mathrm{D_s^+}$ mesons was compared to that of prompt $\mathrm{D_s^+}$ [19] and non-prompt $\mathrm{D^0}$ [21] mesons measured at the same centre-of-mass energy per nucleon pair. The prompt and non-prompt $\mathrm{D_s^+}$ R_{AA} are compared in the top- and bottom-left panels of Fig. 6 for the 0–10% and 30–50% centrality class, respectively. Analogously, the comparison between the nuclear modification factor of non-prompt $\mathrm{D_s^+}$ and non-prompt $\mathrm{D^0}$ mesons is reported in the right panels of the same figure. The R_{AA} of prompt and non-prompt D mesons shows a decreasing trend with increasing p_{T} up to a minimum of about 0.2 (0.4) around 10 GeV/c in the 0–10% (30–50%) centrality class. In the lowest p_{T} intervals, the R_{AA} increases up to unity. In particular, the central values of the non-prompt $\mathrm{D_s^+}$ R_{AA} are higher with respect to those of prompt $\mathrm{D_s^+}$ and non-prompt $\mathrm{D^0}$ in the 0–10% centrality class for $p_{\mathrm{T}} < 6$ GeV/c, even though they are compatible within uncertainties. This possible difference between prompt and non-prompt $\mathrm{D_s^+}$ R_{AA} would be consistent with the different loss of energy experienced by charm and beauty quarks traversing the QGP. In fact, the effect due to the different decay kinematics of charm and beauty hadrons is found to be negligible, as discussed in Ref. [21]. Instead, the difference between non-

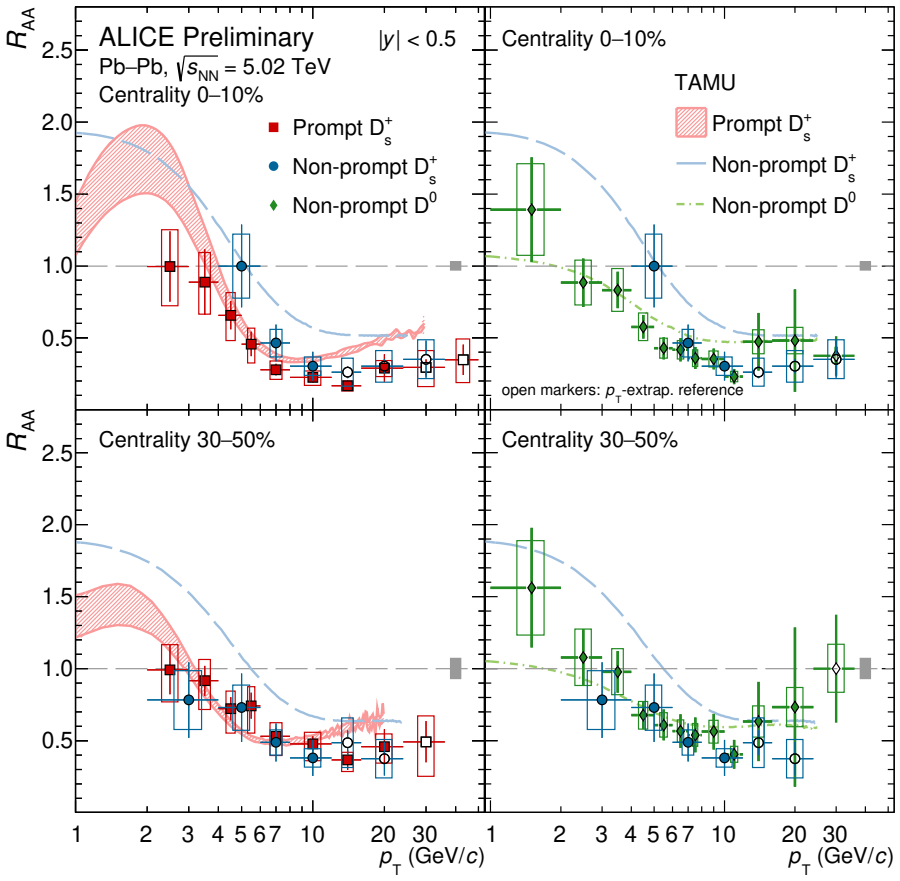

Fig. 6: Left panels: prompt (Ref. [19]) and non-prompt D_s^+-meson R_{AA} in central (top) and semicentral (bottom) Pb–Pb collisions at $\sqrt{s_{NN}} = 5.02$ TeV. Right panels: non-prompt D_s^+- and D^0-meson (Ref. [21]) R_{AA} in central (top) and semicentral (bottom) Pb–Pb collisions at $\sqrt{s_{NN}} = 5.02$ TeV. The experimental results are compared with the predictions of the TAMU model [66]. Statistical (bars), systematic (boxes), and normalisation (shaded box around unity) uncertainties are shown.

prompt D_s^+ and D^0 mesons could result from the hadronisation via recombination and the presence of a strangeness-rich environment. In semicentral collisions, no separation among the R_{AA} of prompt D_s^+, non-prompt D_s^+, and non-prompt D^0 is observed within the measurement uncertainties.

The R_{AA} measurements were compared with the predictions of the TAMU model [66]. In the TAMU model, the heavy-quark transport is described via the Langevin equation and the hadronisation can occur both via recombination with light quarks from the medium, which is the dominant mechanism at low p_T, or via fragmentation, which becomes more important at high p_T. The TAMU predictions are shown in Fig. 6. The uncertainty band for prompt D_s^+ mesons is due to the modification of the parton distribution functions in Pb nuclei, which is neglected for the beauty-quark production. The TAMU model qualitatively describes the p_T trend of the non-prompt D_s^+-meson R_{AA}, although it overestimates the measurements.

In the left and right panels of Fig. 7, the nuclear modification factors of non-prompt D_s^+ mesons divided by that of prompt D_s^+ mesons and non-prompt D^0 mesons are shown, respectively. The measurements in both centrality intervals are compared with the predictions of the TAMU model. In the 0–10% centrality class, the non-prompt D_s^+ to prompt D_s^+ R_{AA} ratio suggests a hint of enhancement with a statistical significance of 1.6σ in the $4 < p_T < 12$ GeV/c interval, which is by construction the same of that reported for the corresponding yield ratio. The R_{AA} ratio is consistent with a larger energy loss for

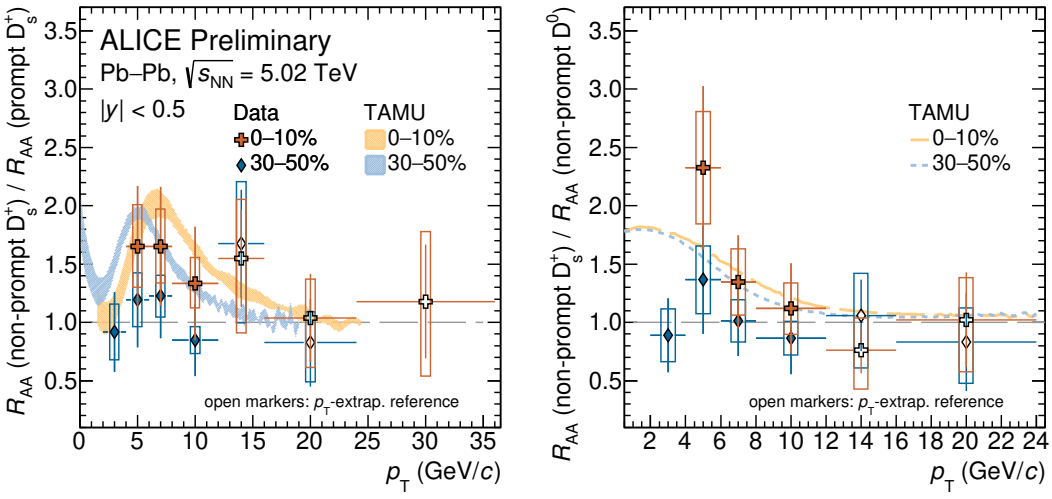

Fig. 7: The R_{AA} of non-prompt D_s^+ mesons divided by the one of prompt D_s^+ mesons [19] (left panel) and non-prompt D^0 mesons [21] (right panel) for the 0–10% and 30–50% centrality intervals in Pb–Pb collisions at $\sqrt{s_{NN}} = 5.02$ TeV. The measurements are compared with TAMU model predictions [66]. Statistical (bars) and systematic (boxes) uncertainties are shown.

the charm quark with respect to the beauty quark due to its smaller mass, as already suggested by the results shown in Fig. 6. No hint for a ratio of the R_{AA} larger than unity is observed in semicentral collisions. Considering the measurement uncertainties, TAMU predictions qualitatively describe the results for central collisions. At variance, for semicentral collisions the TAMU model overestimates the R_{AA} ratio values. The measurements of the non-prompt D_s^+ to non-prompt D^0 R_{AA} ratio suggest a possible enhancement with respect to unity in the $4 < p_T < 12$ GeV/c interval for central collisions, as reported for the yield ratio. In this case, the rise at low p_T might be a consequence of the abundance of strange quarks thermally produced in the QGP and the dominance of the hadronisation via recombination in this range of momentum. The TAMU model describes the data within the experimental uncertainties.

5 Conclusions

In this Note, the first measurement of the non-prompt D_s^+-meson production at midrapidity in Pb–Pb collisions at $\sqrt{s_{NN}} = 5.02$ TeV was reported.

The non-prompt D_s^+-meson production yield was measured between 4 and 36 (2 and 24) GeV/c in the 0–10% (30–50%) centrality interval. These measurements were compared to the ones performed for prompt D_s^+ and non-prompt D^0 mesons at the same centre-of-mass energy. The production yield was employed to compute the non-prompt D_s^+-meson R_{AA}, which was compared with the R_{AA} of prompt D_s^+ and non-prompt D^0 mesons.

The non-prompt D_s^+ R_{AA} shows a significant p_T dependence. A minimum at intermediate transverse momentum ($p_T \approx 10$ GeV/c) around 0.2 (0.4) in central (semicentral) collisions, and a mild increase with decreasing p_T, with R_{AA} reaching (close to) unity at $p_T \approx 4$–6 (2–4) GeV/c in the 0–10% (30–50%) centrality interval are reported. The TAMU model, which implements the parton in-medium energy loss through collisional processes as well as the beauty-quark hadronisation both via fragmentation and recombination, describes the p_T trend of the R_{AA}. However, it overestimates the measurements. Further comparisons were performed between prompt and non-prompt D_s^+ as well as non-prompt D^0 mesons by computing the ratios of their production yields and R_{AA}. These ratios suggest the presence of an enhancement of non-prompt D_s^+ mesons compared to prompt D_s^+ (non-prompt D^0) mesons in central

collisions in the $4 < p_{\mathrm{T}} < 12$ GeV/c interval, with a significance of 1.6σ (1.7σ). The increase is consistent with expectations for the overall effect of the energy-loss mechanism and the hadronisation-process modification in presence of the colour-deconfined medium.

The recent upgrade of the ALICE apparatus will greatly enhance the physics potential of the experiment in the LHC Run 3 data-taking period, allowing for more precise measurements of the non-prompt $\mathrm{D_s^+}$-meson production in heavy–ion collisions.

References

[1] F. Karsch, "Lattice simulations of the thermodynamics of strongly interacting elementary particles and the exploration of new phases of matter in relativistic heavy ion collisions", *J. Phys. Conf. Ser.* **46** (2006) 122–131, arXiv:hep-lat/0608003.

[2] S. Borsanyi, Z. Fodor, J. N. Guenther, R. Kara, S. D. Katz, P. Parotto, A. Pasztor, C. Ratti, and K. K. Szabo, "QCD Crossover at Finite Chemical Potential from Lattice Simulations", *Phys. Rev. Lett.* **125** no. 5, (2020) 052001, arXiv:2002.02821 [hep-lat].

[3] **HotQCD** Collaboration, A. Bazavov *et al.*, "Chiral crossover in QCD at zero and non-zero chemical potentials", *Phys. Lett. B* **795** (2019) 15–21, arXiv:1812.08235 [hep-lat].

[4] U. W. Heinz and M. Jacob, "Evidence for a new state of matter: An Assessment of the results from the CERN lead beam program", arXiv:nucl-th/0002042.

[5] **BRAHMS** Collaboration, I. Arsene *et al.*, "Quark gluon plasma and color glass condensate at RHIC? The Perspective from the BRAHMS experiment", *Nucl. Phys. A* **757** (2005) 1–27, arXiv:nucl-ex/0410020.

[6] **PHOBOS** Collaboration, B. B. Back *et al.*, "The PHOBOS perspective on discoveries at RHIC", *Nucl. Phys. A* **757** (2005) 28–101, arXiv:nucl-ex/0410022.

[7] **STAR** Collaboration, J. Adams *et al.*, "Experimental and theoretical challenges in the search for the quark gluon plasma: The STAR Collaboration's critical assessment of the evidence from RHIC collisions", *Nucl. Phys. A* **757** (2005) 102–183, arXiv:nucl-ex/0501009.

[8] **PHENIX** Collaboration, K. Adcox *et al.*, "Formation of dense partonic matter in relativistic nucleus-nucleus collisions at RHIC: Experimental evaluation by the PHENIX collaboration", *Nucl. Phys. A* **757** (2005) 184–283, arXiv:nucl-ex/0410003.

[9] **ALICE** Collaboration, S. Acharya *et al.*, "Transverse momentum spectra and nuclear modification factors of charged particles in pp, p-Pb and Pb-Pb collisions at the LHC", *JHEP* **11** (2018) 013, arXiv:1802.09145 [nucl-ex].

[10] **ALICE** Collaboration, J. Adam *et al.*, "Anisotropic flow of charged particles in Pb-Pb collisions at $\sqrt{s_{\mathrm{NN}}} = 5.02$ TeV", *Phys. Rev. Lett.* **116** no. 13, (2016) 132302, arXiv:1602.01119 [nucl-ex].

[11] P. Braun-Munzinger, V. Koch, T. Schäfer, and J. Stachel, "Properties of hot and dense matter from relativistic heavy ion collisions", *Phys. Rept.* **621** (2016) 76–126, arXiv:1510.00442 [nucl-th].

[12] M. H. Thoma and M. Gyulassy, "Quark Damping and Energy Loss in the High Temperature QCD", *Nucl. Phys. B* **351** (1991) 491–506.

[13] E. Braaten and M. H. Thoma, "Energy loss of a heavy fermion in a hot plasma", *Phys. Rev. D* **44** (1991) 1298–1310.

[14] E. Braaten and M. H. Thoma, "Energy loss of a heavy quark in the quark - gluon plasma", *Phys. Rev. D* **44** no. 9, (1991) R2625.

[15] R. Baier, Y. L. Dokshitzer, A. H. Mueller, S. Peigné, and D. Schiff, "Radiative energy loss and p_{T} broadening of high-energy partons in nuclei", *Nucl. Phys. B* **484** (1997) 265–282, arXiv:hep-ph/9608322.

[16] M. Gyulassy and M. Plumer, "Jet Quenching in Dense Matter", *Phys. Lett. B* **243** (1990) 432–438.

[17] **ALICE** Collaboration, "Centrality determination in heavy ion collisions", *ALICE-PUBLIC-2018-011* (Aug, 2018) . https://cds.cern.ch/record/2636623.

[18] **ALICE** Collaboration, S. Acharya *et al.*, "Prompt D^0, D^+, and D^{*+} production in Pb–Pb collisions at $\sqrt{s_{\mathrm{NN}}}$ = 5.02 TeV", *JHEP* **01** (2022) 174, arXiv:2110.09420 [nucl-ex].

[19] **ALICE** Collaboration, S. Acharya *et al.*, "Measurement of prompt $\mathrm{D_s}^+$-meson production and azimuthal anisotropy in Pb–Pb collisions at $\sqrt{s_{\mathrm{NN}}} = 5.02$ TeV", *Phys. Lett. B* **827** (2022) 136986, arXiv:2110.10006 [nucl-ex].

[20] **ALICE** Collaboration, S. Acharya *et al.*, "Constraining hadronization mechanisms with $\Lambda_{\mathrm{c}}^+/\mathrm{D}^0$ production ratios in Pb-Pb collisions at $\sqrt{s_{\mathrm{NN}}} = 5.02$ TeV", arXiv:2112.08156 [nucl-ex].

[21] **ALICE** Collaboration, S. Acharya *et al.*, "Measurement of beauty production via non-prompt D^0 mesons in Pb-Pb collisions at $\sqrt{s_{\mathrm{NN}}}$ = 5.02 TeV", arXiv:2202.00815 [nucl-ex].

[22] **CMS** Collaboration, A. M. Sirunyan *et al.*, "Nuclear modification factor of D^0 mesons in PbPb collisions at $\sqrt{s_{\mathrm{NN}}} = 5.02$ TeV", *Phys. Lett. B* **782** (2018) 474–496, arXiv:1708.04962 [nucl-ex].

[23] **CMS** Collaboration, A. M. Sirunyan *et al.*, "Measurement of the $B^{\pm}$ Meson Nuclear Modification Factor in Pb-Pb Collisions at $\sqrt{s_{\mathrm{NN}}} = 5.02$ TeV", *Phys. Rev. Lett.* **119** no. 15, (2017) 152301, arXiv:1705.04727 [hep-ex].

[24] **CMS** Collaboration, A. M. Sirunyan *et al.*, "Measurement of prompt and nonprompt charmonium suppression in PbPb collisions at 5.02 TeV", *Eur. Phys. J. C* **78** no. 6, (2018) 509, arXiv:1712.08959 [nucl-ex].

[25] **CMS** Collaboration, A. M. Sirunyan *et al.*, "Studies of Beauty Suppression via Nonprompt D^0 Mesons in Pb-Pb Collisions at $\sqrt{s_{\mathrm{NN}}} = 5.02$ TeV", *Phys. Rev. Lett.* **123** no. 2, (2019) 022001, arXiv:1810.11102 [hep-ex].

[26] **CMS** Collaboration, A. M. Sirunyan *et al.*, "Measurement of $\mathrm{B_s^0}$ meson production in pp and PbPb collisions at $\sqrt{s_{\mathrm{NN}}} = 5.02$ TeV", *Phys. Lett. B* **796** (2019) 168–190, arXiv:1810.03022 [hep-ex].

[27] **CMS** Collaboration, A. M. Sirunyan *et al.*, "Production of Λ_{c}^+ baryons in proton-proton and lead-lead collisions at $\sqrt{s_{\mathrm{NN}}} = 5.02$ TeV", *Phys. Lett. B* **803** (2020) 135328, arXiv:1906.03322 [hep-ex].

[28] **ALICE** Collaboration, J. Adam *et al.*, "Measurement of electrons from beauty-hadron decays in p-Pb collisions at $\sqrt{s_{\mathrm{NN}}} = 5.02$ TeV and Pb-Pb collisions at $\sqrt{s_{\mathrm{NN}}} = 2.76$ TeV", *JHEP* **07** (2017) 052, arXiv:1609.03898 [nucl-ex].

[29] **STAR** Collaboration, J. Adam *et al.*, "Centrality and transverse momentum dependence of D^0-meson production at mid-rapidity in Au+Au collisions at $\sqrt{s_{\mathrm{NN}}} = 200\,\mathrm{GeV}$", *Phys. Rev. C* **99** no. 3, (2019) 034908, arXiv:1812.10224 [nucl-ex].

[30] Y. L. Dokshitzer, V. A. Khoze, and S. I. Troian, "On specific QCD properties of heavy quark fragmentation ('dead cone')", *J. Phys. G* **17** (1991) 1602–1604.

[31] **ALICE** Collaboration, S. Acharya *et al.*, "Direct observation of the dead-cone effect in QCD", arXiv:2106.05713 [nucl-ex].

[32] B. Svetitsky, "Diffusion of charmed quarks in the quark-gluon plasma", *Phys. Rev. D* **37** (1988) 2484–2491.

[33] **ALICE** Collaboration, S. Acharya *et al.*, "Transverse-momentum and event-shape dependence of D-meson flow harmonics in Pb–Pb collisions at $\sqrt{s_{\mathrm{NN}}}$ = 5.02 TeV", *Phys. Lett. B* **813** (2021) 136054, arXiv:2005.11131 [nucl-ex].

[34] A. Beraudo *et al.*, "Extraction of Heavy-Flavor Transport Coefficients in QCD Matter", *Nucl. Phys. A* **979** (2018) 21–86, arXiv:1803.03824 [nucl-th].

[35] J. Rafelski and B. Muller, "Strangeness Production in the Quark - Gluon Plasma", *Phys. Rev. Lett.* **48** (1982) 1066. [Erratum: Phys. Rev. Lett. 56, 2334 (1986)].

[36] P. Koch, B. Muller, and J. Rafelski, "Strangeness in Relativistic Heavy Ion Collisions", *Phys. Rept.* **142** (1986) 167–262.

[37] **STAR** Collaboration, J. Adam *et al.*, "Observation of $D_{\mathrm{s}}^{\pm}/D^0$ enhancement in Au+Au collisions at $\sqrt{s_{\mathrm{NN}}}$ = 200 GeV", *Phys. Rev. Lett.* **127** (2021) 092301, arXiv:2101.11793 [hep-ex].

[38] **ALICE** Collaboration, S. Acharya *et al.*, "Measurement of $\mathrm{D^0}$, $\mathrm{D^+}$, $\mathrm{D^{*+}}$ and $\mathrm{D_s^+}$ production in Pb–Pb collisions at $\sqrt{s_{\mathrm{NN}}} = 5.02$ TeV", *JHEP* **10** (2018) 174, arXiv:1804.09083 [nucl-ex].

[39] **CMS** Collaboration, A. Tumasyan *et al.*, "Observation of $\mathrm{B_s^0}$ mesons and measurement of the $\mathrm{B_s^0/B^+}$ yield ratio in PbPb collisions at $\sqrt{s_{\mathrm{NN}}}$ = 5.02 TeV", arXiv:2109.01908 [hep-ex].

[40] **STAR** Collaboration, J. Adam *et al.*, "First measurement of Λ_c baryon production in Au+Au collisions at $\sqrt{s_{\mathrm{NN}}}$ = 200 GeV", *Phys. Rev. Lett.* **124** no. 17, (2020) 172301, arXiv:1910.14628 [nucl-ex].

[41] **ALICE** Collaboration, J. Adam *et al.*, "J/ψ suppression at forward rapidity in Pb–Pb collisions at $\sqrt{s_{\mathrm{NN}}} = 5.02$ TeV", *Phys. Lett. B* **766** (2017) 212–224, arXiv:1606.08197 [nucl-ex].

[42] **ALICE** Collaboration, S. Acharya *et al.*, "Studies of J/ψ production at forward rapidity in Pb–Pb collisions at $\sqrt{s_{\mathrm{NN}}}$ = 5.02 TeV", *JHEP* **02** (2020) 041, arXiv:1909.03158 [nucl-ex].

[43] **ALICE** Collaboration, S. Acharya *et al.*, "Centrality and transverse momentum dependence of inclusive J/ψ production at midrapidity in Pb–Pb collisions at $\sqrt{s_{\mathrm{NN}}}$ = 5.02 TeV", *Phys. Lett. B* **805** (2020) 135434, arXiv:1910.14404 [nucl-ex].

[44] **Particle Data Group** Collaboration, P. Zyla *et al.*, "Review of Particle Physics", *PTEP* **2020** no. 8, (2020) 083C01.

[45] **ALICE** Collaboration, S. Acharya *et al.*, "Measurement of beauty and charm production in pp collisions at $\sqrt{s}$ = 5.02 TeV via non-prompt and prompt D mesons", *JHEP* **05** (2021) 220, arXiv:2102.13601 [nucl-ex].

[46] **ALICE** Collaboration, K. Aamodt *et al.*, "Alignment of the ALICE Inner Tracking System with cosmic-ray tracks", *JINST* **5** (2010) P03003, arXiv:1001.0502 [physics.ins-det].

[47] J. Alme *et al.*, "The ALICE TPC, a large 3-dimensional tracking device with fast readout for ultra-high multiplicity events", *Nucl. Instrum. Meth. A* **622** (2010) 316–367, arXiv:1001.1950 [physics.ins-det].

[48] A. Akindinov *et al.*, "Performance of the ALICE Time-Of-Flight detector at the LHC", *Eur. Phys. J. Plus* **128** (2013) 44.

[49] **ALICE** Collaboration, E. Abbas *et al.*, "Performance of the ALICE VZERO system", *JINST* **8** (2013) P10016, arXiv:1306.3130 [nucl-ex].

[50] **ALICE** Collaboration, B. Abelev *et al.*, "Performance of the ALICE Experiment at the CERN LHC", *Int. J. Mod. Phys.* **A29** (2014) 1430044, arXiv:1402.4476 [nucl-ex].

[51] **ALICE** Collaboration, J. Adam *et al.*, "Centrality dependence of the charged-particle multiplicity density at midrapidity in Pb-Pb collisions at $\sqrt{s_{\rm NN}}$ = 5.02 TeV", *Phys. Rev. Lett.* **116** no. 22, (2016) 222302, arXiv:1512.06104 [nucl-ex].

[52] C. Loizides, J. Kamin, and D. d'Enterria, "Improved Monte Carlo Glauber predictions at present and future nuclear colliders", *Phys. Rev. C* **97** no. 5, (2018) 054910, arXiv:1710.07098 [nucl-ex]. [Erratum: Phys.Rev.C 99, 019901 (2019)].

[53] D. d'Enterria and C. Loizides, "Progress in the Glauber Model at Collider Energies", *Ann. Rev. Nucl. Part. Sci.* **71** (2021) 315–344, arXiv:2011.14909 [hep-ph].

[54] T. Chen and C. Guestrin, "Xgboost: A scalable tree boosting system", *Proceedings of the 22nd ACM SIGKDD International Conference on Knowledge Discovery and Data Mining* (2016) 785–794, arXiv:1603.02754 [cs.LG].

[55] L. Barioglio, F. Catalano, M. Concas, P. Fecchio, F. Grosa, F. Mazzaschi, and M. Puccio, "hipe4ml/hipe4ml", July, 2021. https://doi.org/10.5281/zenodo.5070132.

[56] X.-N. Wang and M. Gyulassy, "Hijing: A monte carlo model for multiple jet production in pp, pA, and AA collisions", *Phys. Rev. D* **44** (Dec, 1991) 3501–3516.

[57] T. Sjostrand, S. Mrenna, and P. Z. Skands, "PYTHIA 6.4 Physics and Manual", *JHEP* **05** (2006) 026, arXiv:hep-ph/0603175.

[58] T. Sjöstrand, S. Ask, J. R. Christiansen, R. Corke, N. Desai, P. Ilten, S. Mrenna, S. Prestel, C. O. Rasmussen, and P. Z. Skands, "An introduction to PYTHIA 8.2", *Comput. Phys. Commun.* **191** (2015) 159–177, arXiv:1410.3012 [hep-ph].

[59] P. Skands, S. Carrazza, and J. Rojo, "Tuning PYTHIA 8.1: the Monash 2013 Tune", *Eur. Phys. J. C* **74** no. 8, (2014) 3024, arXiv:1404.5630 [hep-ph].

[60] R. Brun, F. Bruyant, F. Carminati, S. Giani, M. Maire, A. McPherson, G. Patrick, and L. Urban, *GEANT: Detector Description and Simulation Tool; Oct 1994*. CERN Program Library. CERN, Geneva, 1993. http://cds.cern.ch/record/1082634. Long Writeup W5013.

[61] M. Cacciari, M. Greco, and P. Nason, "The $p_{\rm T}$ spectrum in heavy-flavor hadroproduction", *JHEP* **05** (1998) 007, arXiv:hep-ph/9803400 [hep-ph].

[62] M. Cacciari, S. Frixione, and P. Nason, "The $p_{\rm T}$ spectrum in heavy-flavor photoproduction", *JHEP* **03** (2001) 006, arXiv:hep-ph/0102134 [hep-ph].

[63] M. He and R. Rapp, "Hadronization and Charm-Hadron Ratios in Heavy-Ion Collisions", *Phys. Rev. Lett.* **124** no. 4, (2020) 042301, arXiv:1905.09216 [nucl-th].

[64] **ALICE** Collaboration, J. Adam *et al.*, "Transverse momentum dependence of D-meson production in Pb-Pb collisions at $\sqrt{s_{NN}} = 2.76$ TeV", *JHEP* **03** (2016) 081, arXiv:1509.06888 [nucl-ex].

[65] **ALICE** Collaboration, "ALICE 2017 luminosity determination for pp collisions at $\sqrt{s}$ = 5 TeV", *ALICE-PUBLIC-2018-014* (Nov, 2018) . http://cds.cern.ch/record/2648933.

[66] M. He, R. J. Fries, and R. Rapp, "Heavy Flavor at the Large Hadron Collider in a Strong Coupling Approach", *Phys. Lett. B* **735** (2014) 445–450, arXiv:1401.3817 [nucl-th].

[67] W. Ke, Y. Xu, and S. A. Bass, "Linearized Boltzmann-Langevin model for heavy quark transport in hot and dense QCD matter", *Phys. Rev. C* **98** no. 6, (2018) 064901, arXiv:1806.08848 [nucl-th].